UV-vis and IR spectroscopic characterization of diphenyl disulfide radical cation in acid zeolites and its rearrangement to thianthrenium radical cation

Vicente Martí,[a] Lorenzo Fernández,[a] Vicente Fornés,[a] Hermenegildo García *[a] and Heinz D. Roth *[b]†

[a] *Instituto de Tecnología Química CSIC-UPV, Universidad Politécnica de Valencia, Apartado 22012, 46071 Valencia, Spain*
[b] *Department of Chemistry, Wright-Rieman Laboratories, Rutgers University, New Brunswick, New Jersey 08854-8087, USA*

Received (in Gainesville, FL) 18th August 1998, Accepted 7th December 1998

Adsorption of diphenyl disulfide (DPDS) from CH_2Cl_2 solutions onto acid zeolites at room temperature generated the "extended" radical cation, $DPDS^{\bullet+}$. At loadings of 3 wt%, oxidation to $DPDS^{\bullet+}$ is essentially complete. Upon heating the loaded zeolite to 200 °C, the adsorbed $DPDS^{\bullet+}$ was converted into thianthrenium radical cation ($TH^{\bullet+}$). *Ab initio* calculations at the B3LYP and HF levels using the 6-31G* basis set suggest cyclization of a diphenyl disulfide-*S*,*S*-dication as a reasonable rate-determining step of the conversion. Non-acidic zeolites devoid of Lewis and Brønsted sites (as determined by the pyridine adsorption–desorption method) failed to generate $DPDS^{\bullet+}$ to an extent detectable spectroscopically; these results support Lewis and/or Brønsted sites as being responsible for the observed oxidation.

Introduction

Numerous organic radical cations have been generated spontaneously by inclusion of their precursors into zeolites.[1–11] In many cases, these rigid microporous solids provide excellent matrices to stabilize these otherwise very reactive intermediates.[12,13] The remarkable stabilization within the zeolite host arises from the combined contribution of the intense electrostatic fields inside the zeolite and from geometrical restrictions that impede the approach of external reagents.

Much of the previous work in this field has been limited to characterizing the sequestered radical cations and to probing the influence of the zeolite physicochemical parameters on radical cation generation. Studies describing the conversion of a primary radical cation into a well-defined secondary species are rare. A good example of such a conversion is observed upon incorporation of thiophene or thiophene oligomers (*e.g.*, terthiophene) into zeolites. Upon standing or mild heating, the initially formed (oligo-) thiophene radical cations were oxidized to the corresponding dications or, by coupling to a second species with dehydrogenation, to sexithiophene dication.[14]

The ability of zeolites to act as electron acceptors has been ascribed to the presence of Lewis[8,11] or Brønsted acid sites;[12,15,16] however, some zeolites also have been reported to generate radical cations in the Na^+-form.[14,17] These assignments appear incompatible, unless two different mechanisms of radical cation formation are postulated. Na^+ zeolites should be essentially non-acidic; unsolvated Na^+ ions within dehydrated zeolites can act only as weak Lewis sites. However, some adventitious acidity may develop during the calcination of hydrated samples even for *de novo* synthesized Na^+-zeolites; therefore, *de novo* synthesis of a zeolite in the Na^+-form does not ensure *per se* the total absence of acid sites. Of course, adventitious acid sites can be suppressed, and any zeolite sample neutralized, by exhaustive Na^+ exchange.

In this paper, we report the formation of the radical cation ($DPDS^{\bullet+}$) of diphenyl disulfide (DPDS) upon incorporation into a high silica pentasil zeolite (ZSM-5) or mordenite (Mor). The oxidation was observed only in acidic zeolites but failed to occur in non-acidic ZSM-5 samples. Upon heating the loaded zeolite samples, $DPDS^{\bullet+}$ rearranged into the known thianthrenium radical cation ($TH^{\bullet+}$). The radical cations, $DPDS^{\bullet+}$ and $TH^{\bullet+}$ were characterized by diffuse reflectance and IR spectra; the formation of TH was demonstrated by product studies. *Ab initio* quantum chemical calculations provided an approximate wavelength for the absorption maximum of $DPDS^{\bullet+}$ and supported a reaction mechanism involving the diphenyl disulfide dication, $DPDS^{2+}$.

Results and discussion

Adsorption of DPDS from dichloromethane solution onto thermally dehydrated samples of Na-ZSM-5, H-ZSM-5 and H-Mor powders caused the colorless suspension to turn light blue. After washing and evaporation of the solvent the loaded zeolite samples showed diffuse reflectance (DR) spectra featuring an intense peak at 240 nm as well as a very broad low-intensity band, extending from 600 to 1500 nm (Fig. 1). Interestingly, a non-acidic zeolite (Na-ZSM-5–NaCl) remained colorless; the corresponding DR spectrum showed no absorption at long wavelengths. Based on a recent EPR study of DPDS adsorbed on Na-ZSM-5, which showed the presence of $DPDS^{\bullet+}$,[18] we assign the DR spectrum (Fig. 1) as that of $DPDS^{\bullet+}$.

The UV-vis absorption spectra of many organic radical cations are known.[19] In general, these spectra are significantly different from those of their neutral precursors. Open shell configurations introduce new electronic transitions of much lower energies, appearing in the visible or even the near-IR (NIR). Therefore, the observation of significant spectral shifts is considered to be strong evidence for the formation of radical cations.[19]

Radical cations of sulfur containing substrates can be generated conveniently by dissolving the parent compound in con-

† Profesor Visitante IBERDROLA de Ciencia y Tecnología.

centrated sulfuric acid.[20] For example, dissolving TH in H_2SO_4 generated $TH^{\bullet+}$, which slowly decomposed by aromatic sulfonation and overoxidation. However, attempts to obtain the optical spectrum of $DPDS^{\bullet+}$ have, so far, met with failure. Treatment of DPDS with concentrated sulfuric acid or other Lewis and Brønsted acids only generated $TH^{\bullet+}$.[21,22] This transformation was rationalized by a mechanism involving protonation of DPDS.[21] Thiophenol also gave rise to $TH^{\bullet+}$,[21] possibly *via* $DPDS^{\bullet+}$. The $DPDS^{\bullet+}$ radical cation was invoked as an intermediate in the oxidative polymerization of DPDS.[23–26] Apparently, $DPDS^{\bullet+}$ is a highly reactive species in solution, regardless of whether it is generated by chemical,[27,28] photochemical[29] or electrochemical oxidation.[24]

Recently, one of us observed the formation of $DPDS^{\bullet+}$ upon incorporation of DPDS into Na-ZSM-5 at room temperature.[18] The resulting EPR spectrum showed the simultaneous presence of $DPDS^{\bullet+}$ and $TH^{\bullet+}$. This observation agrees with previous EPR studies of DPDS in strong Lewis acids, which showed two sets of signals, one clearly corresponding to $TH^{\bullet+}$, the other one unassigned.[30]

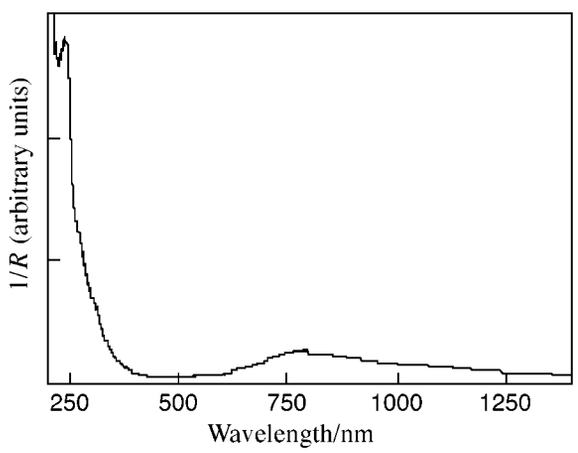

Fig. 1 Diffuse reflectance spectrum (plotted as the inverse of the reflectance, $1/R$) of Na-ZSM-5 zeolite after incorporation of DPDS.

In order to obtain additional support for the assignment of the DR spectrum in Fig. 1 to $DPDS^{\bullet+}$, we carried out *ab initio* calculations at the B3LYP level using the 6-31G* basis set. The optimized geometry of DPDS was used as input for $DPDS^{\bullet+}$. The optimized geometries of DPDS (top) and $DPDS^{\bullet+}$ (bottom) and other relevant parameters are shown in Fig. 2. The calculations predict that the two phenyl rings are orthogonal for DPDS, but are nearly coplanar in $DPDS^{\bullet+}$. The major conformational change upon one-electron oxidation is highly relevant for the incorporation of DPDS into pentasil zeolites: the model predicts a relaxation in the unfavorable van der Waals interaction between host and guest upon conversion of DPDS to $DPDS^{\bullet+}$ (Fig. 3).

However, it is well known that *ab initio* methods may not predict accurately the orbital energies of open-shell configurations; thus, their application to estimate the wavelength of the maximum in the electronic absorption spectrum of a radical cation is limited. For this reason, semiempirical MOPAC calculations were carried out on the B3LYP optimized geometry to estimate the absorption maximum in the optical spectrum of $DPDS^{\bullet+}$. The lowest-energy electronic transition predicted by MOPAC for the doublet, $DPDS^{\bullet+}$, lies in the NIR region, with $\lambda_{max} = 1402$ nm. Given that the experimental band at long wavelength is very broad and has no well-defined maximum ($\lambda_{max} \sim 850$ nm), the calculated value is considered compatible with the experimental band extending to 1450 nm; it certainly is reasonably close in energy.

The FT-IR spectrum of the zeolite samples also provided useful evidence. Although zeolites have a strong absorption near 1100 cm^{-1} (Si–O stretching vibration) as well as weaker overtones in the 2100–1800 cm^{-1} region, some spectral windows exist where the IR bands of the embedded guests can be recorded. In particular, the region characteristic for aromatic stretching vibrations is free from interference. This is important because DR spectroscopy tends to overestimate colored species ($DPDS^{\bullet+}$) and is biased against colorless compounds (DPDS). FT-IR spectroscopy, on the other hand, provides more balanced information about the fraction of DPDS converted to $DPDS^{\bullet+}$ and the fraction of unchanged DPDS inside the zeolites.

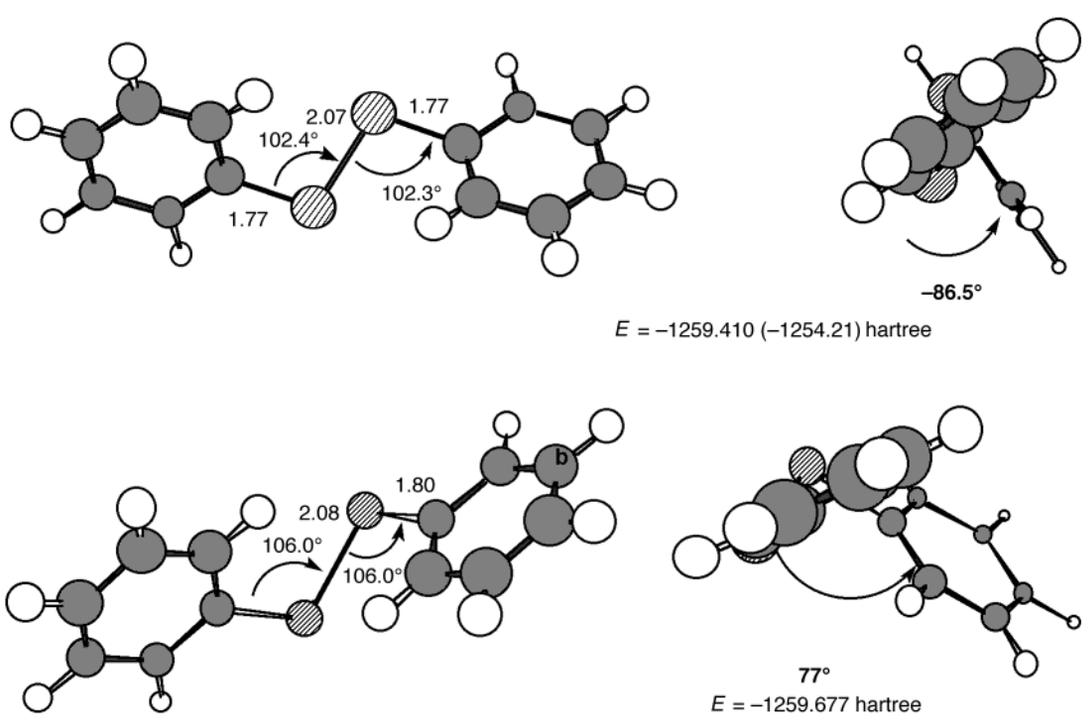

Fig. 2 Optimized geometries at the B3LYP level of DPDS (top) and $DPDS^{\bullet+}$ (bottom). The energies at the HF level are indicated in parentheses. The dihedral angles between the *ipso* and *ortho* carbons of the two phenyl groups are shown in bold.

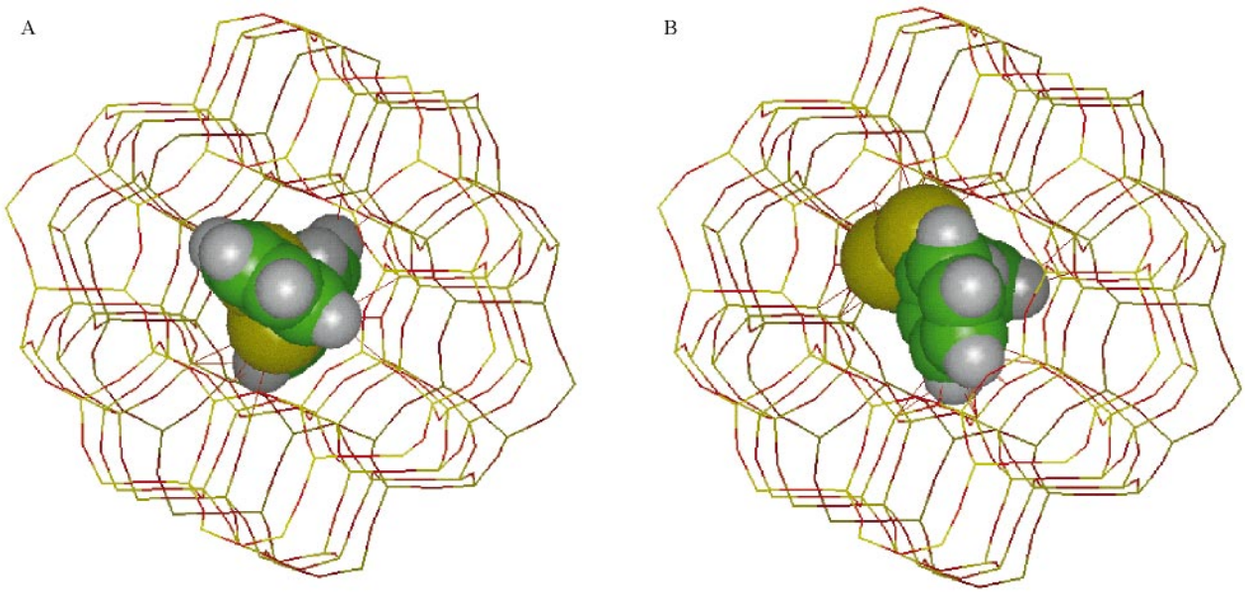

Fig. 3 Molecular modeling visualization of the docking of DPDS (A) and DPDS$^{\bullet+}$ (B) inside the straight channels of ZSM-5.

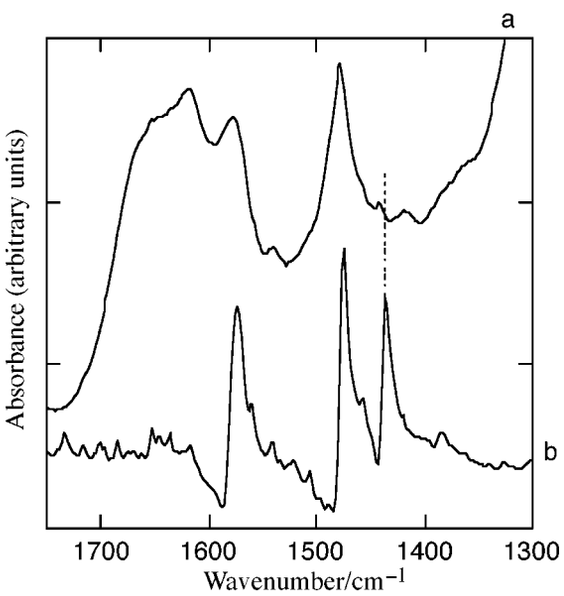

Fig. 4 Aromatic region of the FT-IR spectra of pure DPDS in a KBr disk at room temperature (b) and DPDS adsorbed on H-ZSM-5 (a) after degassing at 100 °C under 10^{-2} Pa for 1 h.

The FT-IR spectrum of the blue H-ZSM-5 sample after incorporation of DPDS (Fig. 4a) and that of DPDS in a KBr disk (Fig. 4b) show remarkable differences in the aromatic region. In addition, minor, but reproducible shifts in the position of the bands near 1480 cm^{-1} were observed. The characteristic sharp band of DPDS (1435 cm^{-1}) is almost completely absent in the blue zeolite sample, indicating the purity of the radical cation inside the zeolite: the lack of absorption at 1435 cm^{-1} is clear evidence that little neutral DPDS remains unreacted. At loadings of *ca.* 3 wt% measured by C and S combustion chemical analysis, oxidation of DPDS to its radical cation is essentially complete according to FT-IR. This may have been expected in view of the relatively low oxidation potential of DPDS (E_{ox} = 1.70 V *vs.* SCE)[31] and given the fact that donors of similar oxidation potential (*viz.*, thianthrene, E_{ox} = 1.71 V *vs.* SCE)[32,33] also were converted completely to radical cations upon adsorption on H-ZSM-5 or analogous zeolites.[13] A spectrum essentially identical to Fig. 4a, was observed upon incorporation of DPDS into H-Mor, indicating an analogous conversion in this zeolite.

Nature of the redox active site

The nature of the redox active site in the zeolite is of significant interest. The ability of zeolites to act as electron acceptors has been ascribed to the presence of Lewis[8,11] or Brønsted acid sites.[12,15,16] Therefore, we probed the efficiency of four zeolites of different acidities. In addition to a *de novo* synthesized Na-ZSM-5[34] and a thoroughly neutralized sample (Na-ZSM-5–NaCl; two consecutive treatments of *de novo* synthesized Na-ZSM-5 with an aqueous 1 M NaCl solution, buffered to pH 8.5), the efficiency of two acidic zeolites, H-ZSM-5 and H-mordenite (H-Mor), was tested. FT-IR analysis showed external ≡Si–OH groups as well as residual bridging ≡Si–(OH)–Al≡ hydroxy groups in all samples, except the carefully neutralized one. The latter hydroxy groups are considered responsible for the Brønsted acidity in zeolites. The Lewis and Brønsted acidity of our samples has been assessed by the pyridine adsorption–desorption method. The IR spectra of the samples showed the characteristic vibration bands associated with the pyridinium ion (1550 cm^{-1}) and the pyridine Lewis adduct (1450 cm^{-1}); the relative intensities of these bands are a measure of the number of Lewis and Brønsted sites, respectively (Fig. 5).

Significantly, all but the thoroughly neutralized sample converted DPDS to DPDS$^{\bullet+}$. These results clearly show that the *de novo* synthesized Na-ZSM-5 was acidic and its ability to generate radical cations disappeared as soon as the residual acidity was neutralized by further Na^+ exchange. The data presented in Fig. 5 do not allow, however, differentiation between Lewis and Brønsted sites as the seat of electron acceptor capacity, because the pyridine adsorption method established that both types of site are present simultaneously in the three active zeolites.

In this context, it is interesting to note that the formation of *trans*- and *cis*-1,3-dianisylbut-1-ene upon adsorption of vinylanisole on Na–Y was attributed to an acid-catalyzed dimerization due to adventitious acid sites within the zeolite.[35] Similarly, low levels of Brønsted acidity were recently identified in Na–X and Na–Y zeolites by spectral changes due to the conversion of retinyl Schiff base to its protonated form.[36]

Thermal isomerization of DPDS$^{\bullet+}$

The thermal stability of DPDS$^{\bullet+}$ was evaluated by heating samples of blue H-Mor and H-ZSM-5 zeolites containing DPDS progressively up to 200 °C under nitrogen. Starting at 150 °C, a change in the color of the zeolite powders from blue

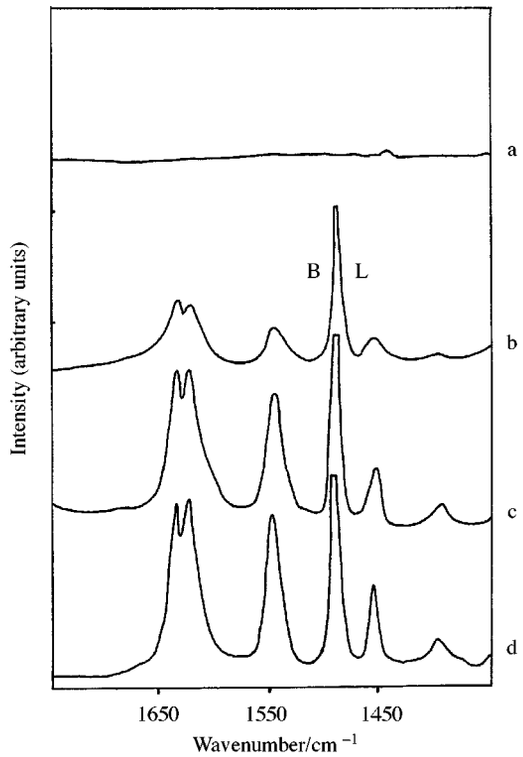

Fig. 5 Infrared spectra of pyridine adsorbed on (a) Na-ZSM-5–NaCl, (b) as-synthesized Na-ZSM-5, (c) H-ZSM-5, and (d) H-Mor, after pyridine vapor adsorption at room temperature and subsequent desorption at 250 °C for 1 h. The bands characteristic of Lewis and Brønsted acid sites are labeled L and B, respectively.

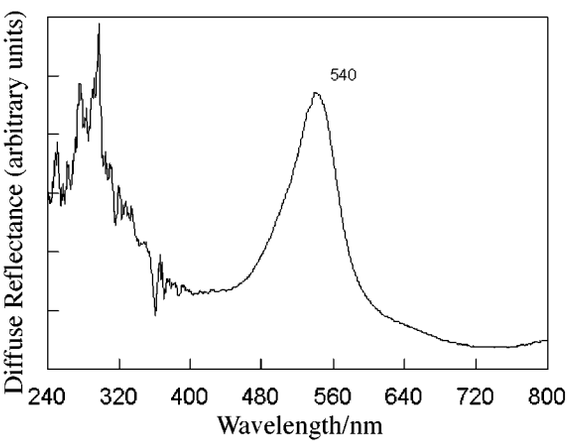

Fig. 6 Diffuse reflectance spectrum (plotted as the inverse of the reflectance, $1/R$) of DPDS–H-ZSM-5 after heating the sample to 170 °C at a rate of 15 °C min^{-1}.

to pink became apparent. The UV-vis DR spectra of the samples (Fig. 6) showed an intense band centered at 540 nm, matching the known optical spectrum of $TH^{\bullet+}$ inside zeolites.[13] $TH^{\bullet+}$ is stable under these conditions.[12] The conversion of $DPDS^{\bullet+}$ to $TH^{\bullet+}$ was confirmed by an intense IR absorption band at 1518 cm^{-1}; a band at this wavelength has been observed in the FT-IR of authentic $TH^{\bullet+}$ in acid zeolites,[12] and is absent in either DPDS or $DPDS^{\bullet+}$. Finally, refluxing a suspension of DPDS in CH_2Cl_2 in the presence of H-ZSM-5 yielded TH as the only product together with unreacted DPDS. These results clearly show that $DPDS^{\bullet+}$ undergoes a clean thermal rearrangement to $TH^{\bullet+}$ inside the zeolite.

A plausible reaction mechanism for the observed conversion is outlined in Scheme 1. The radical cation, $DPDS^{\bullet+}$, is the logical first intermediate in any oxidation of DPDS, although this intermediate has been elusive in solution and only recently

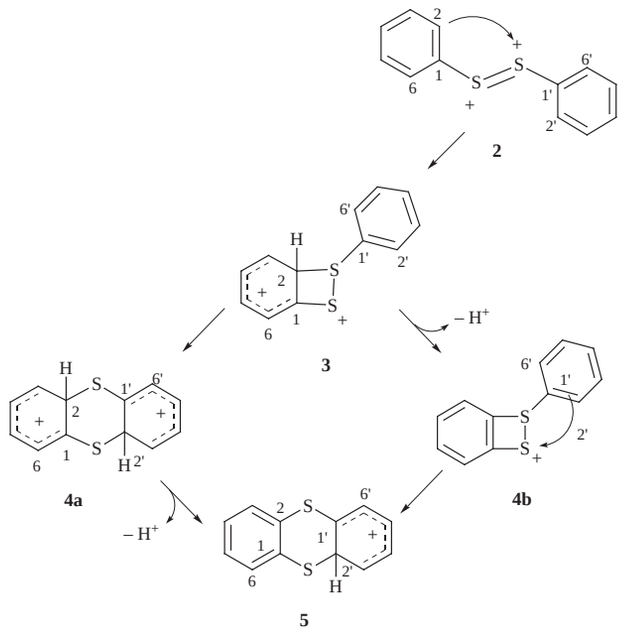

Scheme 1 Key intermediates considered for the rearrangement of $DPDS^{\bullet+}$ into $TH^{\bullet+}$.

has been observed in ZSM-5.[18] The DR and IR results discussed above clearly support the formation of $DPDS^{\bullet+}$ in H-ZSM-5 and H-Mor. Upon heating, $DPDS^{\bullet+}$ undergoes a second electron transfer, forming the disulfur dication, $DPDS^{2+}$, which is considered to be the key intermediate in this conversion.

Dipositive disulfur species are not without precedent; for example, dialkyl disulfide dications have been identified by photoelectron spectroscopy; their involvement was also concluded based on conductivity measurements following pulse radiolysis.[37] These experiments were interpreted as evidence for disproportionation of disulfide radical cation, at an essentially diffusion controlled rate, forming neutral disulfide and dication. The disproportionation is favored by the formation of a sulfur–sulfur double bond in the dication. Dipositive disulfur species have been proposed also in the oxygenation of related sulfur heterocycles.[38] In the zeolite-induced conversion discussed here we have excluded bimolecular processes from consideration, as molecules and intermediates most likely assume extended conformations and have limited mobility. Instead, we assume two consecutive one-electron oxidations, which have precedent in zeolites. The considerable activation indicated by the conversion temperature need not indicate a significantly higher second oxidation potential. It may simply reflect the energy required for migration of $DPDS^{\bullet+}$ to a sufficiently active zeolite site.

Overall, the conversion of DPDS to $TH^{\bullet+}$ involves the loss of three electrons and two protons, a net conversion equivalent to the generation of anethole radical cation from *p*-propylanisole observed recently.[39] However, unlike the oxidation/deprotonation of the anisole derivative, the conversion of $DPDS^{2+}$ (**2**) to $TH^{\bullet+}$ requires two intramolecular electrophilic aromatic additions, aside from the final one-electron oxidation of TH to $TH^{\bullet+}$. The first addition involves cyclization, whereas the second occurs with ring expansion. We have considered two variations for this conversion, involving either alternating addition and deprotonation (the sequence **2**, **3**, **4b**, **5**) or two successive additions followed by two successive deprotonations (the sequence **2**, **3**, **4a**, **5**).

Ab initio calculations

To study the viability of the proposed mechanism, *ab initio* calculations of the reaction intermediates of Scheme 1 were

Table 1 Calculated bond lengths (Å) of selected intermediates in the conversion of DPDS to thianthrenium ion

Species	C^1–C^2	C^1–C^6	C^1–S^1	S^1–S^2	S^2–$C^{1'}$	$C^{1'}$–$C^{2'}$	S^1–$C^{2'}$	S^2–C^2
DPDS	1.40	1.40	1.80	2.08	1.80	1.40	3.34[a]	3.34[a]
$DPDS^{\bullet+}$	1.41	1.41	1.77	2.07	1.77	1.41	3.27[a]	3.27[a]
2, $DPDS^{2+}$	1.42	1.43	1.74	2.03	1.73	1.42	3.27[a]	3.27[a]
$\mathbf{3}^{(2+)}$	1.49	1.39	1.72	2.25	1.73	1.42	4.44[a]	1.92
$\mathbf{4a}^{(2+)}$	1.50	1.49	1.73	3.56[a]	1.73	1.50	1.73	1.73
$\mathbf{4b}^{(+)}$	1.39	1.39	1.80	2.21	1.77	1.40	4.32[a]	1.80
$\mathbf{5}^{(+)}$	1.41	1.40	1.78	3.36[a]	1.70	1.50	1.86	1.78

[a] Non-bonding distances.

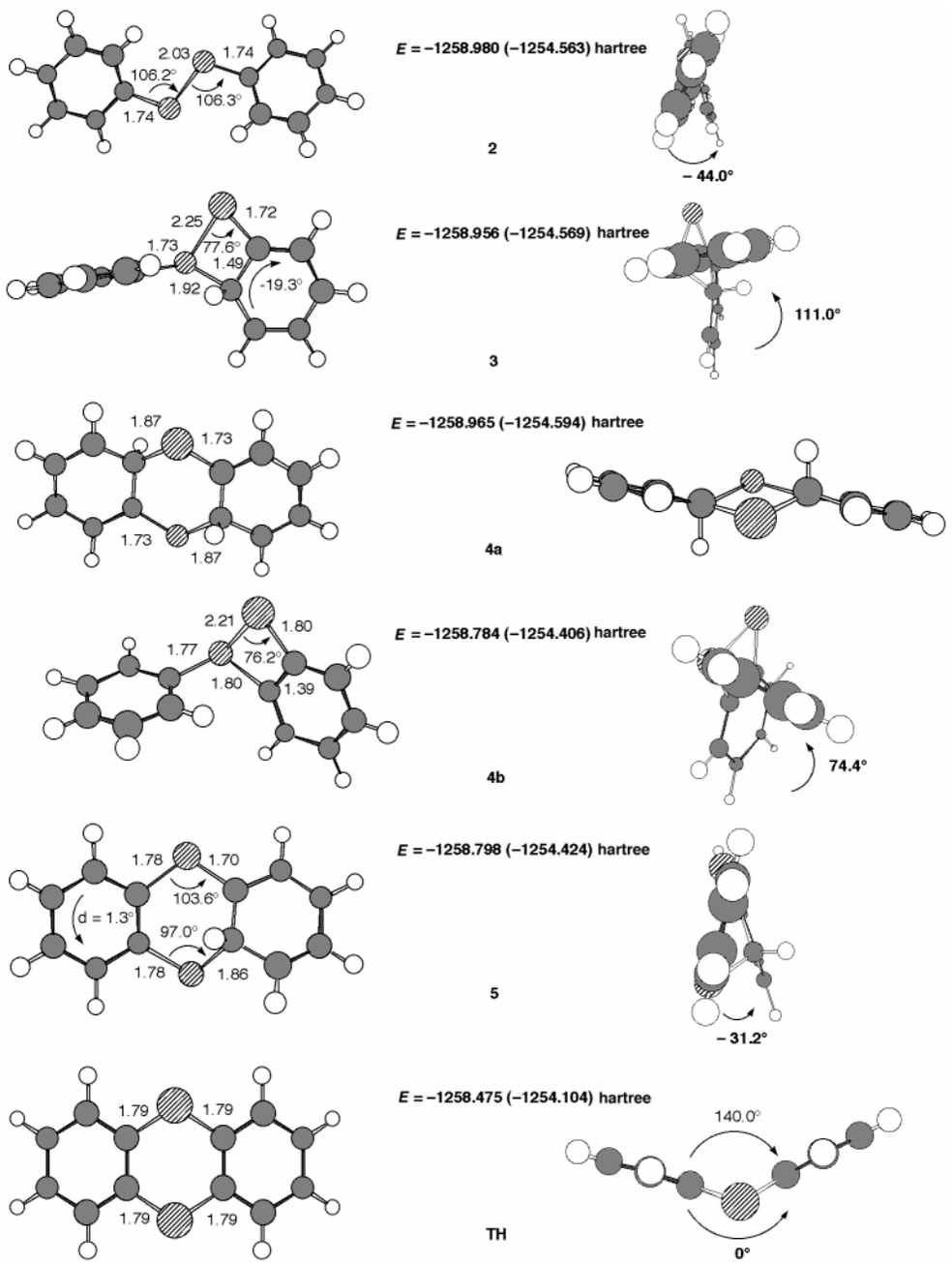

Fig. 7 Optimized geometries and energies at the B3LYP level of theory for potential reaction intermediates **2**–**5** and TH. The energy at the HF level is indicated in parentheses. The dihedral angles between the *ipso* and *ortho* carbons of the pairs of phenyl and/or cyclohexadienyl groups are shown in bold.

carried out at the HF and B3LYP levels using the 6-31G* basis set. The optimized geometries are shown in Fig. 7; some of the salient parameters are presented in Tables 1–3. Taking into account that this rearrangement occurs inside a restricted reaction cavity, one key consideration concerns the change in the geometry of the reaction intermediates, and whether these species can be accommodated inside the zeolite channels. Particularly the orientation of the two phenyl substituents, diagnosed by comparing the dihedral angle defined by their normal axes, appears to be of crucial significance.

Table 2 Calculated bond angles (degrees) of intermediates in the conversion of DPDS to thianthrenium ion

Species	$\angle C^2–C^1–S^1$	$\angle C^6–C^1–S^1$	$\angle C^1–S^1–S^2$	$\angle S^1–S^2–C^{1'}$	$\angle S^2–C^{1'}–C^{2'}$	$\angle S^2–C^{1'}–C^{6'}$	$\angle C^{1'}–S^2–C^2$	$\angle C^1–S^1–C^{2'}$
DPDS	124.3	115.6	106.0	106.0	124.3	115.6	—	—
$DPDS^{\bullet+}$	123.0	115.6	102.4	102.3	123.0	115.6	—	—
2, $DPDS^{2+}$	126.0	112.3	106.2	106.3	126.0	112.3	—	—
$\mathbf{3}^{(2+)}$	106.5	132.0	77.6	113.9	113.0	125.0	111.6	—
$\mathbf{4a}^{(2+)}$	119.2	117.3	—	—	123.0	108.0	104.6	104.7
$\mathbf{4b}^{(+)}$	104.4	134.8	76.2	110.7	115.0	122.8	108.6	—
$\mathbf{5}^{(+)}$	122.6	118.5	—	—	121.2	118.3	105.6	97.0

Table 3 Calculated dihedral angles (degrees) of potential intermediates in the conversion of DPDS to thianthrenium ion

Species	$\angle C^1–S^1–S^2–C^{1'}$	$\angle C^2–C^1–C^{1'}–C^{2'}$	$\angle C^6–C^1–C^{1'}–C^2$	$\angle C^5–C^6–C^1–C^2$	$\angle C^6–C^1–C^{1'}–C^{6'}$	$\angle C^3–C^2–C^1–S^1$
DPDS	93.9	−73.0	136.3	−0.7	−73.7	−177.8
$DPDS^{\bullet+}$	155.5	95.2	−94.2	0.5	76.3	−177.7
2, $DPDS^{2+}$	162.5	139.0	−42.6	1.6	136.2	178.4
$\mathbf{3}^{(2+)}$	121.7	−92.6	−91.2	10.3	92.2	153.8
$\mathbf{4a}^{(2+)}$	108.5	24.5	−88.9	−0.3	100.3	−178.9
$\mathbf{4b}^{(+)}$	−179.5	179.7	78.6	−8.5	180.0	−177.2
$\mathbf{5}^{(+)}$	154.9	143.9	36.9	−0.7	136.8	−180.0

We had shown previously that the pore dimensions of pentasil zeolites are adequate to accommodate the products, TH and $TH^{\bullet+}$.[12] Likewise, adsorption experiments indicate that DPDS can be included inside the channels of ZSM-5. Therefore, we focussed our study on the "docking" of the intervening reaction intermediates, **2**–**5**, inside the zeolite pores. The results suggest that the overall conversion is feasible, although a small degree of van der Waals overlap between host and guest is predicted for intermediates **3**–**5**. Particularly the conversion of dication **2** to **3** may present something of a steric problem; the attack of sulfur converts the planar phenyl ring of species **2** to a potentially more bulky cyclohexadienyl moiety in the resulting dication **3**.

However, this is not expected to pose a problem, because the conversion was carried out at elevated temperatures, where the minor steric impediments can be overcome. An increase in temperature typically facilitates the diffusion and other motions of the adsorbate by increasing its kinetic energy and the vibrational frequency of the lattice. Even molecules with more significant mismatches have been incorporated into zeolites at elevated temperatures. For example, C_{60} was incorporated into Y zeolite, even though its molecular diameter (7.9 Å) is larger than that of the zeolite supercage (7.4 Å).[40]

The intermediates of the reaction sequence in Scheme 1 are part of the hypersurface representing the reaction mechanism. Each pair of intermediates is separated by a barrier (transition state) which determines their rate of interconversion and the overall reaction rate. In view of the size of the molecules discussed here and considering the computational resources required for the calculation of the transition states we have limited our calculations to the free energies (and structures) of the intermediates. The formation of the intermediate with the largest increase in free energy is assumed to be rate determining. Of course, this step can be assigned only with caution; particularly, the direct comparison of closed-shell and open-shell intermediates may be seriously flawed. The total free energies of the reaction intermediates calculated at the B3LYP/6-31G* levels are included in Fig. 7.

The pathway proceeding *via* successive electrophilic additions involves three consecutive (closed shell) dications, **2**, **3** and **4a**; the free energies of these species can be compared directly. The first electrophilic aromatic addition, generating **3** from **2**, is significantly endergonic ($\Delta E = +0.024263$ hartrees, 15.2 kcal mol^{-1}); this step is the most endergonic reaction considered in Scheme 1. The free energy increase is not surprising; it can be ascribed to the strain energy in the resulting four-membered ring combined with the loss of aromaticity. The second aromatic addition, forming **4a**, is mildly exergonic ($\Delta E = -0.008701$ hartrees, −5.45 kcal mol^{-1}). The decrease in free energy shows that the relief of ring strain outweighs the loss of aromaticity. For the formation of **5** from **4a**, a comparison of their energies is possible only if a proton acceptor and its conjugate acid are included. We chose the silyl ether, $H_3Si–O–SiH_3$ (−657.881328 hartrees), to simulate the framework oxygens that presumably act as basic centers in the deprotonation, and its conjugate acid, the oxonium ion, $H_3Si–(^+OH)–SiH_3$ (−658.183028 hartrees). Adding the corresponding energies to those of **4a** and **5** results in an energy difference, $\Delta E = -0.134737$ hartrees (−84.2 kcal mol^{-1}), for the conversion.

The pathway proceeding *via* alternating addition and deprotonation is also initiated by the (endergonic) conversion of **2** to **3**. The formation of **4b** from **3** again requires including $H_3Si–O–SiH_3$ and $H_3Si–(^+OH)–SiH_3$ as base and conjugate acid. This results in an energy difference, $\Delta E = -0.129474$ (−81.2 kcal mol^{-1}), for the conversion. The second aromatic addition, generating **5** from **4b**, interconverts two (closed shell) monocations; it is exergonic ($\Delta E = -0.013964$ hartrees, −8.5 kcal mol^{-1}), even though it involves the loss of aromaticity. This result reflects the high ring strain in **4b**. Apparently, relief of ring strain more than compensates for the loss of aromaticity.

A comparison of the two pathways (with inclusion of a base and its conjugate acid) shows that deprotonation of **3** (yielding **4b**) is significantly favored over the second aromatic addition (yielding **4a**). Thus, given the well-established presence of proton-acceptor sites in the zeolite,[39] **4b** appears to be the more likely intermediate in the conversion of **3** to **5**. In view of the large free energy difference between deprotonation and aromatic addition (−80 *vs.* −5 kcal mol^{-1}), the actual nature of the proton accepting site does not appear crucial for the course of the reaction; however, such a site must be present and readily accessible.

Conclusion

In summary, $DPDS^{\bullet+}$ has been generated by incorporation of DPDS within acid zeolites; the resulting radical cation was characterized by DR and IR spectroscopies. Non-acidic zeolites (Na-ZSM-5–NaCl) failed to promote the oxidative generation of $DPDS^{\bullet+}$. Upon heating the loaded zeolite samples to temperatures above 150 °C, $DPDS^{\bullet+}$ rearranged to $TH^{\bullet+}$ inside the zeolite pores in a clean and efficient manner. *Ab initio* calculations suggest that the intramolecular electrophilic addition of $DPDS^{2+}$ forming the strained dication, **3**, is the rate determining step in the thermal conversion.

Experimental

Materials

Silica (Ludox AS-40) and alumina gels (Carlo Erba), the NH_4^+-form of mordenite (P.Q., CBV 20A), and DPDS (Aldrich) were commercial samples and used as received.

Na-ZSM-5 was synthesized by hydrothermal crystallization of silica and alumina gels in aqueous basic medium (NaOH) in the absence of a template according to a literature procedure.[34] FT-IR analysis showed external ≡Si–OH groups as well as residual bridging ≡Si–(OH)–Al≡ hydroxy groups (*vide infra*).

The acid sites were neutralized at room temperature by two consecutive treatments of as-synthesized Na-ZSM-5 with aqueous 1 M NaCl solution, adjusted to pH 8.5 with a 0.4 M Na_2CO_3–$NaHCO_3$ buffer, and using a solid to liquid weight ratio of 1-to-10. The resulting zeolite, Na-ZSM-5–NaCl, was washed thoroughly with distilled water to remove residual base introduced by the buffer and dried at 105 °C in air.

Fully protonic H-ZSM-5 was prepared by Na^+-to-NH_4^+ ion exchange of the as-synthesized Na-ZSM-5 by stirring at room temperature consecutively with 0.6 and 1 M solutions of aqueous NH_4OAc, using a solid–liquid weight ratio of 10. The resulting NH_4-ZSM-5 was deep-bed calcined at 500 °C overnight under air.

H-Mor was prepared from a commercial sample of NH_4^+-mordenite by calcination at 500 °C overnight.

Analytical procedures

Chemical analyses of Na and Al were carried out by atomic absorption spectrometry after dissolving known amounts of dehydrated samples in concentrated HF–HNO_3 solutions at 60 °C. Combustion chemical analysis of C and S was carried out using a Perkin-Elmer EA 1108-CHNS-O analyzer.

Diffuse reflectance spectra were recorded in a Cary 5G UV-Vis-NIR spectrophotometer using an integrating sphere attachment and $BaSO_4$ as standard. FT-IR spectra were recorded on a Nicolet spectrophotometer. Zeolite samples (*ca.* 10 mg) were compressed at 1 Ton cm^{-2} under reduced pressure. The resulting self-supporting wafers were placed into a greaseless quartz cell with CaF_2 windows. The samples were outgassed successively at increasing temperatures (100, 200 and 300 °C) under 10^{-2} Pa before recording the IR spectra at room temperature.

The acidity of the zeolite samples was characterized by the pyridine adsorption–desorption method. Pyridine vapor (10^2 Pa) was adsorbed onto dehydrated zeolite wafers at room temperature and subsequently desorbed for 1 h each at 150, 250 and 350 °C under dynamic vacuum. This basic probe molecule can distinguish between Brønsted acid sites (pyridinium ion, 1550 cm^{-1}) and Lewis acid sites (coordinated Lewis adduct, 1450 cm^{-1}).[41–44] Fig. 5 shows the aromatic region of the FT-IR of pyridine adsorbed on the four zeolites used in this study after desorption at 250 °C and 10^{-2} Pa.

Although its chemical analysis is consistent with the Na^+-form (Table 4), the as-synthesized Na-ZSM-5 sample (Fig. 5b) clearly has significant quantities of Lewis acid sites related to the presence of unsolvated Na^+ cation (weak sites), non-framework Al (stronger sites) and, importantly, also Brønsted sites. The latter sites are strong enough to retain a significant fraction of pyridine even after desorption at 350 °C under 10^{-2} Pa for 1 h.

In contrast, the sample which was neutralized by two consecutive treatments of as-synthesized Na-ZSM-5 with aqueous 1 M NaCl solution no longer showed any acid sites (Fig. 5a). The NaCl treatment completely suppressed the residual acidity of the as-synthesized Na-ZSM-5. On the other hand, the fully protonic H-ZSM-5 (Fig. 5c) and H-Mor (Fig. 5d) showed strong Lewis and Brønsted acid sites much larger than those of the as-synthesized Na-ZSM-5. The main analytical and textural parameters of the zeolites used in this work are summarized in Table 4.

Table 4 Relevant analytical and textural data for zeolites used in this work

Zeolite	Si/Al ratio	Na_2O (%)	S_{BET} [a]/ $m^2\ g^{-1}$	Average particle size/ μm
Na-ZSM-5	20	1.97	316	1
Na-ZSM-5–NaCl	20	2.02	316	1
H-ZSM-5	18	0.05	430	1–3
H-Mor	10	<0.02	550	0.3

[a] Specific surface area according to the Brunauer–Emmett–Teller algorithm.

Reaction procedures

The adsorption of DPDS was carried out by stirring solutions of 10 mg DPDS in 15 ml dichloromethane in the presence of 250 mg thermally (500 °C, overnight) dehydrated zeolite for 30 min at room temperature. The suspension was filtered and the solid dried at reduced pressure (≤1 Torr) for 1 h and stored in closed vials.

The thermal rearrangement of $DPDS^{\bullet+}$ was carried out by heating compressed pellets of acid zeolites containing $DPDS^{\bullet+}$ in a tubular oven up to 200 °C under a nitrogen stream at a rate of 10 °C min^{-1}. After this treatment, the zeolites were extracted with CH_2Cl_2 and TH was characterized by GC (Hewlett-

Table 5 Calculated total energies (hartree) of potential intermediates in the conversion of DPDS to thianthrenium ion

Species	HF 6-31G*	Total energy B3LYP/6-31G*	Δ*E*	Species + Si–O–Si B3LYP/6-31G*	Species + Si–(⁺OH)–Si B3LYP/6-31G*	Δ*E*
DPDS						
$DPDS^{\bullet+}$	−1255.0207878	−1259.4101897				
2, $DPDS^{2+}$	−1254.5635663	−1258.9804471	Δ*E* (**2**–**3**)			
			+0.0242631			
3$^{(2+)}$		−1258.956184	Δ*E* (**3**–**4a**)	−1258.956184		
			−0.0087015	−657.881328		
				−1916.837512		
4a$^{(2+)}$		−1258.9648855		−1258.964885		Δ*E* (**3**–**4b**)
				−657.881328		−0.129474
				−1916.846213		
4b$^{(+)}$	−1254.4061701	−1258.783958	Δ*E* (**4b**–**5**)		−1258.783958	
			−0.0139643		−658.183028	
					−1916.966986	
5$^{(+)}$	−1254.4235434	−1258.7979223			−1258.797922	Δ*E* (**4a**–**5**)
					−658.183028	−0.134737
					−1916.980950	

Packard 5890 chromatograph with FID detector equipped with a 25 m capillary column of 5% crosslinked phenylmethylsilicone) and GC-MS (Varian Saturn II, same column as GC) by comparison with an authentic sample.

Calculations

Models and methodology. Calculations were carried out using the GAUSSIAN94 suite of programs.[45] They were performed on a Convex SPP 1000. All structures were optimized without symmetry constraints by two different methods of calculations: i) Hartree–Fock self-consistent field, and ii) electronic correlation by density functional theory methods (DFT),[46] using the B3LYP model.[47] All calculations were performed using the 6-31G* basis set[48] which has d-type polarisation functions on non-hydrogen atoms. The energies and geometries of the radical cations were calculated using open shell configurations.

Acknowledgements

Thanks are due to the Generalidad Valenciana for a scholarship (V. M.) and to the Spanish Ministry of Education for a postdoctoral fellowship (L. F.). H. D. R. gratefully acknowledges the 1997 IBERDROLA Award.

References

1 S. S. Pollack, R. F. Sprecher and E. A. Frommell, *J. Mol. Catal.*, 1991, **66**, 195.
2 C. J. Rhodes, *J. Chem. Soc.*, *Faraday Trans.*, 1991, **87**, 3179.
3 C. J. Rhodes, I. D. Reid and E. Roduner, *J. Chem. Soc.*, *Chem. Commun.*, 1993, 512.
4 C. J. Rhodes, *Colloids Surf. A*, 1993, **72**, 111.
5 R. Crockett and E. Roduner, *J. Chem. Soc.*, *Perkin Trans. 2*, 1993, 1503.
6 C. J. Rhodes and M. Standing, *J. Chem. Soc.*, *Perkin Trans. 2*, 1992, 1455.
7 E. Roduner, R. Crockett and L. M. Wu, *J. Chem. Soc.*, *Faraday Trans.*, 1993, **89**, 2101.
8 F. R. Chen and J. J. Fripiat, *J. Phys. Chem.*, 1992, **96**, 819.
9 E. Baciocchi, G. Doddi, M. Ioele and G. Ercolani, *Tetrahedron*, 1993, **49**, 3793.
10 D. Brunel, J. B. Nagy, G. Daelen, E. G. Derouane, P. Geneste and D. J. Vanderveken, *Appl. Catal. A*, 1993, **99**, 9.
11 F. R. Chen and J. J. Fripiat, *J. Phys. Chem.*, 1993, **97**, 5796.
12 A. Corma, V. Fornes, H. Garcia, V. Marti and M. A. Miranda, *Chem. Mater.*, 1995, **7**, 2136.
13 J. V. Folgado, H. Garcia, V. Marti and M. Espla, *Tetrahedron*, 1997, **53**, 4947.
14 C. V. Casper, V. Ramamurthy and D. R. Corbin, *J. Am. Chem. Soc.*, 1991, **113**, 600.
15 G. A. Ozin and J. Godber, *J. Phys. Chem.*, 1989, **93**, 878.
16 M. L. Cano, A. Corma, V. Fornés and H. García, *J. Phys. Chem.*, 1995, **99**, 4241.
17 V. Ramamurthy, C. V. Casper and D. R. Corbin, *J. Am. Chem. Soc.*, 1991, **113**, 594.
18 P. S. Lakkaraju, D. Zhou and H. D. Roth, *J. Chem. Soc.*, *Perkin Trans. 2*, 1998, 1119.
19 T. Shida, *Electronic Absorption Spectra of Radical Ions*, Verlag Chemie, New York, 1988, vol. 34.
20 A. J. Bard, A. Ledwith and H. J. Shine, *Adv. Phys. Org. Chem.*, 1976, **12**, 155.
21 A. Fava, P. B. Sogo and M. Calvin, *J. Am. Chem. Soc.*, 1957, **79**, 1078.
22 S. Plaza and R. Gruzinski, *Wear*, 1996, **194**, 212.
23 A. C. Archer and P. A. Lovell, *Polymer*, 1995, **36**, 4315.
24 K. Yamamoto, E. Tsuchida, H. Nishida, S. Yoshida and Y. S. Park, *J. Electrochem. Soc.*, 1992, **139**, 2401.
25 E. Tsuchida, K. Yamamoto and H. Nishide, *J. Macromol. Sci.*, *Part A*, 1990, **27**, 1119.
26 E. Tsuchida, K. Yamamoto, M. Jikei, E. Shouji and H. Nishide, *J. Macromol. Sci.*, *Part A*, 1991, **28**, 1285.
27 M. Wejchanjudek and B. Perkowskaspiewak, *Polym. Degrad. Stab.*, 1995, **48**, 131.
28 K. Oyaizu, N. Iwasaki, K. Yamamoto, H. Nishide and E. Tsuchida, *Bull. Chem. Soc. Jpn.*, 1994, **67**, 1456.
29 K. Yamamoto, K. Oyaizu and E. Tsuchida, *Macromol. Chem. Phys.*, 1994, **195**, 3087.
30 J. E. Wertz and J. L. Vivo, *J. Am. Chem. Soc.*, 1955, **77**, 2193.
31 K. Yamamoto, M. Jikei, J. Katoh, H. Nishide and E. Tsuchida, *Macromolecules*, 1992, **25**, 2698.
32 G. Jones, II and B. Huang, *Tetrahedron Lett.*, 1993, 269.
33 G. Jones, II, B. Huang and S. F. Griffin, *J. Org. Chem.*, 1993, **58**, 2035.
34 V. P. Shiralkar and A. Clearfield, *Zeolites*, 1989, **9**, 363.
35 F. L. Cozens, R. Bogdanova, M. Régimbald, H. García, V. Martí and J. C. Scaiano, *J. Phys. Chem. B*, 1997, **101**, 6924.
36 V. J. Rao, D. L. Perlstein, R. J. Robbins, P. H. Lakshminarasimhan, H.-M. Kao, C. P. Grey and V. Ramamurthy, *Chem. Commun.*, 1998, 269.
37 J. Giordan and H. Bock, *Chem. Ber.*, 1982, **115**, 2548.
38 H. J. Shine and D. R. Thompson, *Tetrahedron Lett.*, 1966, 1591.
39 P. S. Lakkaraju, D. Zhou and H. D. Roth, *Chem. Commun.*, 1996, 2605.
40 S. Fukuzumi, T. Suenobu, T. Urano and K. Tanaka, *Chem. Lett.*, 1997, 875.
41 J. W. Ward, *J. Catal.*, 1968, **11**, 238.
42 J. Arribas, A. Corma and V. Fornés, *J. Catal.*, 1984, **88**, 374.
43 A. Corma, *Chem. Rev.*, 1995, **95**, 559.
44 A. Corma, *Chem. Rev.*, 1997, **97**, 2373.
45 M. J. Frisch, G. W. Trucks, H. B. Schlegel, P. M. W. Gill, B. G. Johnson, M. A. Robb, J. R. Cheeseman, T. Keith, G. A. Peterson, J. A. Montgomery, K. Raghavachari, M. A. Al-Laham, V. G. Zakrzewski, J. V. Ortiz, J. B. Foresman, J. Cioslowski, B. B. Stefanov, A. Nanayakkara, M. Challacombe, C. Y. Peng, P. Y. Ayala, W. Chen, M. W. Wong, J. L. Andres, E. S. Replogle, R. Gomperts, R. L. Martin, D. J. Fox, J. S. Binkley, D. J. Defrees, J. Baker, J. P. Stewart, M. Head-Gordon, C. Gonzalez and J. A. Pople, GAUSSIAN 94, Gaussian Inc, Pittsburgh, 1995.
46 P. Hohenberg and W. Kohn, *Phys. Rev. B*, 1964, **136**, 864.
47 C. Lee, W. Yang and R. G. Parr, *Phys. Rev. B*, 1988, **37**, 785.
48 W. J. Hehre, R. Ditchfield and J. A. Pople, *J. Chem. Phys.*, 1972, **56**, 2257.

Paper 8/06522E